Carina Heisig[1]
Christoph Glotzbach[2]
Steffen Schirrmeister[2]
Thomas Turek[1,*]

Selective Hydrogenolysis of Biomass-Derived Xylitol to Glycols: Reaction Network and Kinetics

The conversion of bio-based xylitol to ethylene glycol (EG) and propylene glycol (PG) was studied to replace the petrochemical production route and achieve a sustainable process. The reaction network for aqueous-phase catalytic hydrogenolysis of xylitol over a supported Pt catalyst with $Ca(OH)_2$ as promotor was identified and the reaction kinetics was determined. The effects of reaction conditions such as educt concentration, H_2 pressure, and temperature were investigated. With the developed kinetic model, the composition of the product mixture regarding the desired products (EG, PG) and by-products can be described. The maximum EG yield was achieved at high pressure and low temperature, while high pressure and temperature favored PG production.

Supporting Information available online

1 Introduction

The industrial revolution at the end of the 18th century led to the establishment of fossil fuels (coal, crude oil, and natural gas) as main resources. Today, the majority of chemicals are still produced from these resources, resulting in the consumption of more than 1 billion barrels of oil per year by the chemical industry [1]. Related to this consumption, the emission of huge amounts of carbon dioxide, reaching 33.9 billion tons in 2018, is a major problem [2]. To lower the corresponding environmental impacts, alternative sustainable processes based on renewable resources such as sugars, sugar alcohols, oils, and lignocellulose have become increasingly attractive [3, 4].

Ethylene glycol (EG) and propylene glycol (PG) are high-added-value chemicals and important intermediates in the chemical industry. They are used in polymer chemistry and serve as starting materials for various polymer (intermediate) products. In addition, EG is used as a de-icing agent in the aviation industry, while PG is an excellent carrier for dyes, antioxidants, and enzymes in the chemical, pharmaceutical, cosmetics, and food industries due to its emulsifying properties.

Nowadays, these glycols are produced on the industrial scale (EG: 26.8 million tons in 2017 [5], PG: 1.9 million tons in 2016 [6]) almost exclusively by multi-stage conversion of petroleum-based ethylene and propylene via the respective epoxy intermediate [7–10]. In the production of bio-based EG and PG, glycerol (GLY) has proven to be a promising starting material, which is produced in large quantities as a by-product of biodiesel production (100 kg per ton of biodiesel). However, since biodiesel is obtained from vegetable fats and oils (mainly rapeseed oil, soybean oil, and palm oil), there is competition with the food industry in terms of sustainable use of the cultivated land [11].

In recent years, therefore, the conversion of renewable, non-edible biomass, more precisely lignocellulose, has gained in importance. With a share of 70 %, lignocellulose accounts for the majority of the total global biomass production on land (estimated 170×10^9–200×10^9 t) [12]. As a share of different waste streams, lignocellulose is constantly available, e.g., in agriculture, the timber industry, and the paper industry. It is mainly composed of the natural polymers cellulose, hemicellulose, and lignin, the proportion of which can vary greatly depending on the plant material. By hydrolysis, the polysaccharide hemicellulose can be depolymerized to the monosaccharide xylose. Subsequently, hydrogenation to the sugar alcohol xylitol (XYL) is possible. This in turn can be converted in aqueous solution and under basic conditions to EG and PG [13]. The advantage of this process, compared to the direct conversion of hemicellulose to glycols, is the individual adaptation of the catalysts and reaction conditions for each individual process step. This allows higher selectivities to the two glycols to be achieved.

[1]Carina Heisig, Prof. Dr.-Ing. Thomas Turek
turek@icvt.tu-clausthal.de
Clausthal University of Technology, Institute of Chemical and Electrochemical Process Engineering, Leibnizstrasse 17, 38678 Clausthal-Zellerfeld, Germany.

[2]Dr. Christoph Glotzbach, Dr. Steffen Schirrmeister
thyssenkrupp Industrial Solutions AG, Friedrich-Uhde-Strasse 15, 44141 Dortmund, Germany.

Thus, over the last decade, the production of glycols via catalytic hydrogenolysis of sugars and sugar alcohols has been the subject of intensive development. This resulted in extensive research and development (R&D) efforts on the laboratory and pilot scales, carried out by several companies like thyssenkrupp [14–16], Braskem [17], Avantium [18, 19], and UPM [20], all aiming towards large-scale production. The product distribution of XYL hydrogenation varies with the employed catalysts and operation conditions. Various heterogeneous catalysts and alkaline promotors have been described as highly efficient for the hydrogenolysis of XYL in an aqueous phase. Besides monometallic catalysts containing noble metals, i.e. platinum, ruthenium, copper, cerium, and nickel, as active species, various bimetallic and trimetallic catalysts on different supports, i.e., activated carbon, TiO_2, Al_2O_3, or SiO_2, are mentioned. Examples of these catalysts are Cu/SiO_2 [21, 22], Ni/C [23–25], Ni/Al_2O_3 [26, 27], Ni/TiO_2 [28], Pt/C [25, 29], Ru/C [25, 26, 30–33], $Cu-CaO/Al_2O_3$ [34, 35], $Ni-Cu/SiO_2$ [36], Ni-Re/C [37, 38], Ru-Re/C [34], and Ni-Cu-Ag/C [39], whereby NaOH, KOH, MgO, $Ba(OH)_2$, or $Ca(OH)_2$ were used as basic promotors.

However, little work has been done to predict the reaction conditions of aqueous-phase hydrogenolysis of XYL required to produce an industrially relevant product composition. Therefore, we focus in our study on the identification of the reaction network and the development of the reaction kinetics for the aqueous-phase catalytic hydrogenolysis of XYL over a supported Pt catalyst with $Ca(OH)_2$ as alkaline promotor. We aim to determine the optimum reaction conditions to maximize the yield of the target products (EG and PG). For this purpose, a new kinetic model for the hydrogenolysis of aqueous XYL solutions was developed that allows the quantitative description of the product composition as a function of the educt concentration, the temperature, and the pressure.

2 Experimental

2.1 Materials

XYL ($\geq$ 99.0 wt %), EG ($\geq$ 99.75 wt %), PG ($\geq$ 99.5 wt %), and GLY ($\geq$ 99.5 wt %) were received from Acros Organics whereas lactic acid (LA; $\geq$ 98 wt %) was supplied by Alfa Aesar. Acetic anhydride ($\geq$ 99.0 wt %) and pyridine ($\geq$ 99.5 wt %), used for the acetylation of samples prior to gas chromatography, were obtained from Alfa Aesar. The water used for high-performance liquid chromatography (HPLC) calibrations was supplied by an ultrapure-water device from Sartorius AG (Arium 611VF, 18.2 Ω cm, 0.055 μS cm^{-1} at 25 °C). Water used for the hydrogenation experiments was prepared with a water demineralizer supplied by behr Labor-Technik (behropur® E28dK, 0.5 μS cm^{-1} at 25 °C). The catalyst (5 wt % Pt on activated carbon) was received from Evonik (Noblyst® P2061). It was supplied wet (52.3 wt % H_2O) and did not undergo any pretreatment before usage. A particle diameter of x_{50} = 25 μm was measured with a laser diffraction spectrometer (Sympatec GmbH, type: HELOS/KR). The same instrument was also used to determine the particle diameter of calcium hydroxide ($\geq$ 97.5 wt %, x_{50} = 5 μm) obtained from Acros Organics.

2.2 Hydrogenolysis Experiments

The hydrogenation experiments were carried out in the same laboratory plant supplied by Mothes Hochdrucktechnik GmbH that was described in our previous work [40]. The plant consists of a heatable double-jacket stirred-tank reactor with 4 L volume equipped with an agitator with a magnetic driver, a gassing stirrer, a pressure control system, and a liquid sample line. In addition, a transfer line is connected to the lid of the stirred tank. This enables sampling from the gas phase and its online analysis by gas chromatography.

In a typical run, catalyst powder, calcium hydroxide, and aqueous XYL solution (range: 0.017–0.067 $g_{cat}g_{XYL}^{-1}$) were introduced into the vessel and heated to the set temperature (range: 170–200 °C) under reduced stirring speed (250 rpm), whereby the hydrogen pressure was regulated to the desired value (range: 40–100 bar). The lower stirring speed guaranteed a homogeneous temperature distribution of the reaction solution without dispersing the catalyst particles. After the start-up process, a reactant conversion of up to 13 % was typically observed. After reaching the specified temperature and pressure, the reaction was initiated by increasing the stirring speed to 1000 rpm to avoid mass transfer limitations. During the experiments, the pressure was kept constant by re-dosing the hydrogen consumed by the hydrogenation reactions. For the determination of the reaction network and reaction kinetics of XYL hydrogenolysis, experiments at different pressures, temperatures, reactant concentrations, and amounts of catalyst were conducted.

The liquid samples with a mass of about 6 g (plus 10 g to clean the tubing) taken from the reactor were analyzed using an HPLC device equipped with a refractive index detector tempered at 30 °C and a UV detector (Phenomenex Rezex ROA H$^+$ at 80 °C, 5 mmol L^{-1} H_2SO_4 as mobile phase, flow rate of 0.6 mL min^{-1}, injection volume 5 μL). Moreover, an aliquot of the liquid samples (100 μL) was acetylated for 48 h using a mixture of acetic anhydride and pyridine (3:1 (v/v), 1 mL). The analysis was performed using a 7820A gas chromatograph (GC) from Agilent, equipped with a capillary column (Agilent DB-23) and a flame ionization detector (FID). The gaseous samples were relieved to ambient pressure and analyzed using a second GC (Agilent, type 7890B) equipped with two FID. Due to a special arrangement of the columns, the polar components were analyzed using a capillary column (Agilent, type HP-INNOWax), the nonpolar components with a PLOT column (Agilent, type GS-GasPro), and the permanent gases (e.g., CO, CO_2, methane) with a packed column (Restek, type ShinCarbon) after methanization over a nickel catalyst.

For the analysis of carbonates, a two-necked flask was connected to a dropping funnel via a U-tube (see Sect. S1 in the Supporting Information). Since this is a closed system, no water drips from the dropping funnel into the beaker, which is placed on a balance. At the start of the experiment, hydrochloric acid (HCl) in excess (6 M, ~65 g) is added to the reaction solution (70–80 g) in the two-necked flask via a septum. The hydrochloric acid reacts with the carbonate, forming carbon dioxide. The increase in volume due to CO_2 and HCl displaces an equivalent amount of water from the dropping funnel. If the density of the water is constant, the volume of carbon dioxide

V_{CO_2} can be calculated from the difference between the added amount of acid m_{HCl} and the displaced amount of water m_{H_2O}. The formed amount of carbon dioxide is then determined using the ideal gas law ($T = 20\,°C$, $p = 1.01325\,bar$). Assuming complete mixing, the total amount of CO_2 produced in the reaction n_{CO_2} can be obtained via Eq. (1).[1]

$$n_{CO_2} = \frac{p}{RT}\left(\frac{m_{H_2O}}{\rho_{H_2O}} - V_{HCl}\right)\frac{V_{sol}}{V_{sample}} \tag{1}$$

For a better comparability of the temporal profiles of the remaining educt concentration and yield in dependence on the catalyst amount m_{cat}, the time t is replaced by the modified time t_{mod} (Eq. 2).

$$t_{mod} = \frac{t\,m_{cat}}{V_{sol}} \tag{2}$$

Here, the volume of the reaction solution V_{sol} also takes into account the volume decrease by liquid sampling, while the loss by water evaporation was negligibly small. In addition, the minimal amount of volatile components can also be neglected.

The yield $Y_{p,e}$ is defined as the amount of product p formed during the reaction related to the amount of educt e at the start of the reaction (Eq. 3). Since organic components with variable carbon numbers are formed, the stoichiometry of the reactions is taken into account by the stoichiometric coefficients ν_i and the number of carbon atoms β_i. The mass balance during the hydrogenation experiments is assessed through the sum of the yields (Eq. 4).

$$Y_{p,e} = \frac{c_p - c_{p,0}}{c_{e,0}}\frac{\nu_e}{\nu_p}\frac{\beta_p}{\beta_e} \tag{3}$$

$$\text{mass balance} = \sum Y_{p,e} \tag{4}$$

3   Determination of the Reaction Network

For the determination of the product spectrum during XYL hydrogenolysis, a first experiment with an educt concentration of $0.657\,mol_{XYL}L_{sol}^{-1}$, a catalyst loading of $0.0033\,g_{cat}g_{sol}^{-1}$ and a base concentration of $0.02\,g_{Ca(OH)_2}g_{sol}^{-1}$ was carried out at $170\,°C$ and $80\,bar$. The resulting profiles of product yield and XYL residual as a function of the modified time are shown in Fig. 1. The yield profiles of the gaseous components are shown in Sect. S2 of the Supporting Information (Fig. S2).

It can be seen that XYL was completely consumed after about 16 h ($2.1 \times 10^5\,s\,g_{cat}L_{sol}^{-1}$) with the formation of EG, PG, LA, and GLY as main products. As by-products, the carboxylic acids glycolic, acetic, and formic acid were formed as well as the alcohols methanol, ethanol, n-propanol, and 2-propanol, the ketone acetone, and the polyols 1,2-butanediol, 2,3-butanediol, 1,4-butanediol, 1,2-pentanediol, erythritol, and threitol. In the gas phase, methane, ethane, propane, and butane were detected as well as the evaporated share of methanol, ethanol,

n-propanol, and 2-propanol. The permanent gases CO and CO_2, which were formed during XYL conversion, reacted with calcium hydroxide, forming poorly soluble calcium carbonate. The quantification of the carbonate amount was only possible at the end of the experiment ($Y_{CaCO_3} = 0.02\,mol\,mol^{-1}$). In this experiment, the mass balance was closed, while the mass balance was at least $95.6\,\%$, during all hydrogenation experiments carried out.

Our findings are in good agreement with previous publications [22, 25, 31]. Rivière et al. [31], e.g., observed for a different type of catalyst (2.9 wt % Ru/C), the same catalyst amount ($0.033\,g_{cat}g_{XYL}^{-1}$) and XYL concentration ($0.657\,mol_{XYL}L_{sol}^{-1}$), similar reaction conditions ($200\,°C$, 60 bar instead of $170\,°C$, 80 bar), and a marginally lower $Ca(OH)_2$ amount (0.167 instead of $0.200\,g_{Ca(OH)_2}g_{sol}^{-1}$), an EG selectivity of 28 mol % and a PG selectivity of 25 mol % [31], which are in good agreement with our own measurements corresponding to 33 mol % EG and 29 mol % PG.

In a further series of measurements, the secondary products and intermediates PG, EG, GLY, and LA were also used as reactants. The amount of the respective component previously detected during XYL hydrogenolysis was used as educt concentration, whereby the catalyst amount and the concentration of the solid base were kept constant ($0.0033\,g_{cat}g_{sol}^{-1}$ and $0.02\,g_{Ca(OH)_2}g_{sol}^{-1}$; EG: $0.532\,mol\,L_{sol}^{-1}$, PG: $0.329\,mol\,L_{sol}^{-1}$, GLY: $0.130\,mol\,L_{sol}^{-1}$, and LA: $0.244\,mol\,L_{sol}^{-1}$).

As an example, the results of GLY hydrogenolysis are shown in Fig. 2. The results of the other components (EG, PG, and LA) as well as the results of the gas phase analyses are shown in Sect. S2 of the Supporting Information. As main products of GLY hydrogenolysis, large amounts of PG and LA as well as small amounts of EG were formed. Furthermore, small amounts of by-products, i.e., glycolic acid, methanol, ethanol, n-propanol, and acetone, were produced. In the gas phase, methane, ethane, and propane were detected (see Sect. S2 of the Supporting Information, Fig. S3). The carbonate analysis results in a yield of $0.02\,mol\,mol^{-1}$ at the end of the experiment (reaction time: 44 h).

During hydrogenation of EG, minor amounts of glycolic acid, methanol and ethanol, methane and ethane were detected. The carbonate amount at the end of the experiment was comparatively small ($0.01\,mol\,mol^{-1}$ yield after 44 h of reaction time). Since the mass balance is not closed, it is assumed that non-detectable oligomeric compounds were formed.

During hydrogenation of PG, a small amount of LA was detected ($0.04\,mol\,mol^{-1}$ yield after 44 h of reaction time) as well as minor amounts of ethanol, n-propanol, 2-propanol, methane, ethane, propane, and carbonates. Finally, LA hydrogenation produced small amounts of PG ($0.03\,mol\,mol^{-1}$ yield after 44 h of reaction time), acetone, and methane.

Based on those experiments and work previously published by our project partners [41], we propose the reaction network for XYL hydrogenolysis under basic condition that is shown in Fig. 3. In aqueous solution, there is equilibrium between XYL and its isomeric forms arabitol and ribitol. XYL therefore can be converted via different reaction paths. It is assumed that the hydrogenolysis of XYL to glycolic acid and the unstable intermediate pyruvaldehyde takes place. While glycolic acid reacts to formic acid, the aldehyde is converted to both PG and LA,

---

1)   List of symbols at the end of the paper.
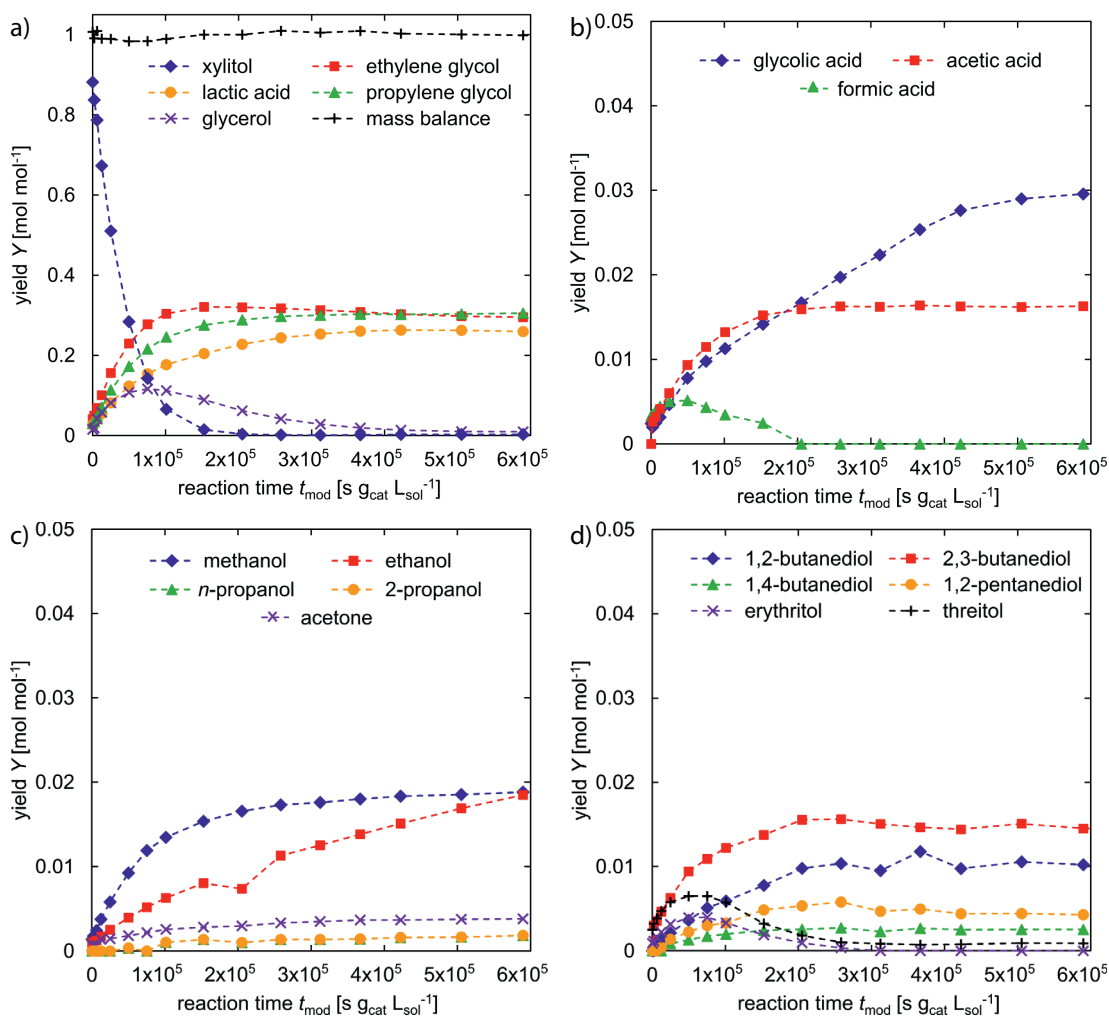
Figure 1. Concentration profiles during hydrogenolysis of aqueous XYL solutions. Reaction conditions: 170 °C, 80 bar, 0.657 $mol_{XYL}L_{sol}^{-1}$, 0.0033 $g_{cat}g_{sol}^{-1}$, 0.02 $g_{Ca(OH)_2}g_{sol}^{-1}$. (a) Main products, (b–d) side products.
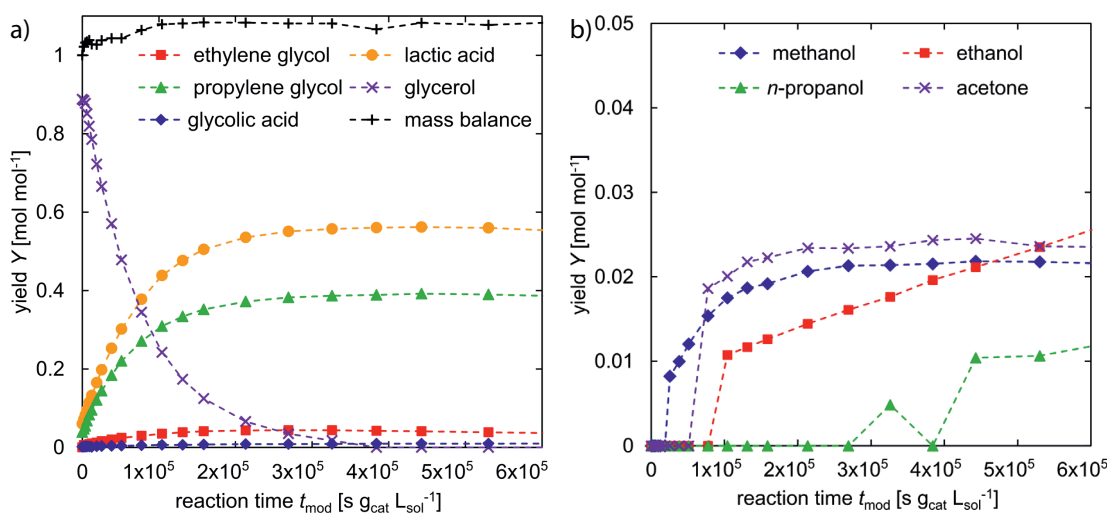
Figure 2. Concentration profiles during hydrogenation of aqueous GLY solutions. Reaction conditions: 170 °C, 80 bar, 0.130 $mol_{GLY}L_{sol}^{-1}$, 0.0033 $g_{cat}g_{sol}^{-1}$, 0.02 $g_{Ca(OH)_2}g_{sol}^{-1}$. (a) Main products, (b) side products.
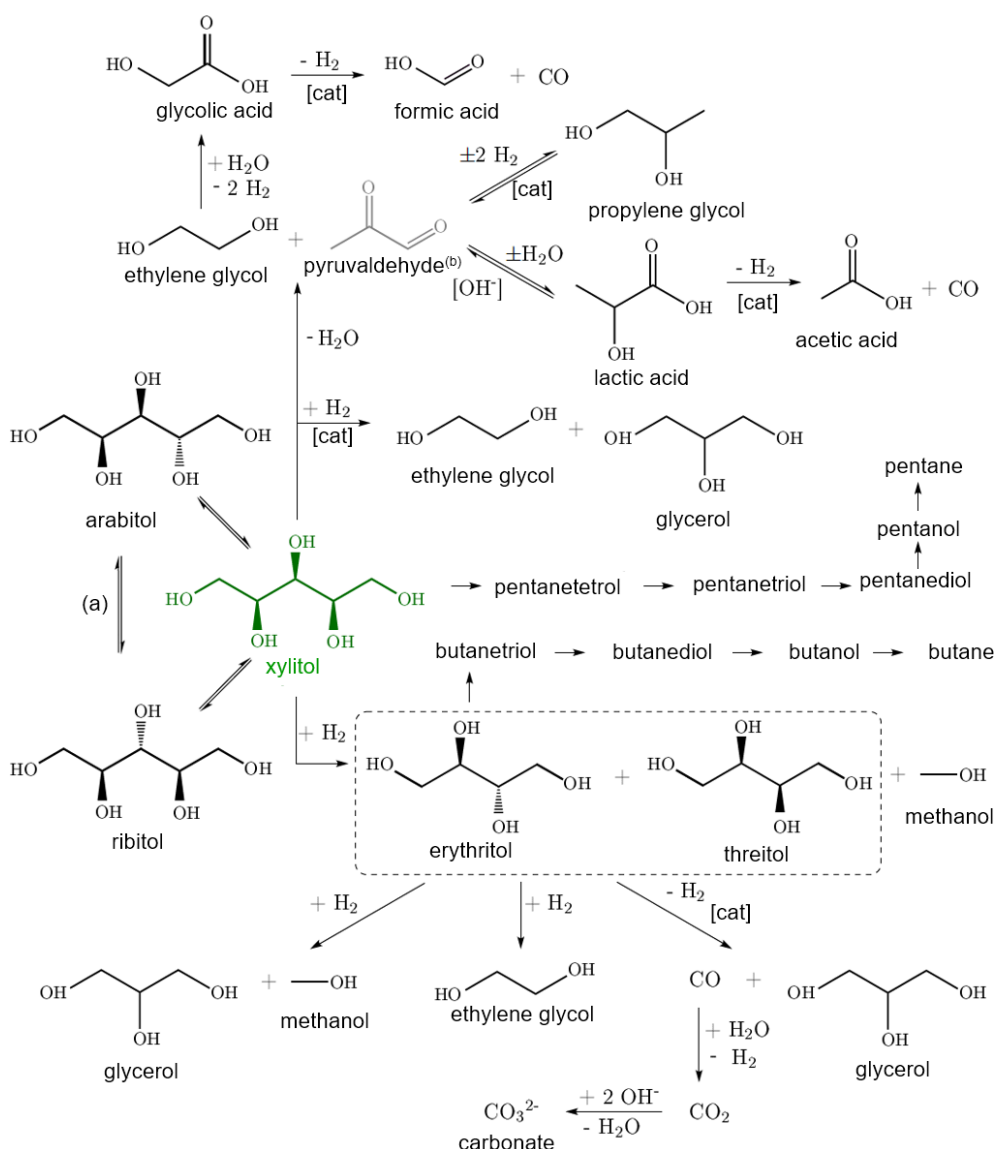
Figure 3. Reaction network for the hydrogenolysis of aqueous XYL solutions. (a) Isomerization of XYL was detected via GC, (b) pyruvaldehyde was assumed to be converted instantly.

which in turn partially reacts to acetic acid. Furthermore, the hydrogenolysis of XYL to EG and GLY takes place as well as the conversion of XYL to the C_4 alcohols erythritol and threitol. Those can react further via different reaction pathways forming methanol, EG, GLY, and carbonate. Finally, the formation of C_5 polyols from XYL takes place, as does the formation of C_4 polyols from erythritol and threitol.

4 Determination of the Reaction Kinetics

For the determination of the reaction kinetics, hydrogen solubility data are required, since most of the reactions take place at the catalyst surface in the liquid phase. As some of the reactions are catalyzed by hydroxide ions, the solubility data of the solid base calcium hydroxide have to be determined, too. Addi-

tionally, it has to be ensured that external and internal mass transport influences are absent, in order to determine the intrinsic kinetics. By adapting the simulated results to the experimentally derived concentration profiles, the parameters of the reaction rate equations (i.e., the rate constants, reaction orders, and inhibition terms) are then determined.

4.1 Determination of the Solubility Data

Since no solubility data of hydrogen in aqueous XYL solutions for the considered ranges of pressure and temperature are available, the solubility data of hydrogen in water were calculated according to Schäfer [42] (see our previous work [40]). This simplification is justified as the solubility of hydrogen in an aqueous XYL solution is comparable to its solubility in

water (see Sect. S3 of the Supporting Information). The hydrogen concentrations for the investigated range of reaction conditions are summarized in Tab. 1.

Table 1. Solubility of hydrogen for the reaction conditions of XYL hydrogenation.

Pressure p [bar]	Solubility of hydrogen [mol L^{-1}] at			
	170 °C	180 °C	190 °C	200 °C
20	0.014	0.013	0.011	0.007
40	0.037	0.039	0.039	0.039
60	0.061	0.065	0.068	0.070
80	0.084	0.091	0.097	0.102
100	0.107	0.117	0.126	0.134

Since there are no data available in the literature on the solubility of calcium hydroxide in aqueous XYL solutions, the solubility data of calcium hydroxide in water were used for kinetic modeling (Tab. 2).

Table 2. Solubility of calcium hydroxide for the reaction conditions of XYL hydrogenation [43, 44].

Temperature T [°C]	Concentration c [mol L^{-1}]
170	0.0042
180	0.0038
190	0.0033
200	0.0029

4.2 Evaluation of the Mass Transport Limitations

With regard to the availability of hydrogen, the possible influence of mass transport limitations was determined for the external mass transfer, using standard Sherwood correlations, and for the internal mass transfer, using a simplified Thiele modulus approach (see our previous work [40]). For simplification, it is assumed that the conversion of XYL is a first-order reaction. In contrast to the procedure described in our previous work, here the catalyst efficiency for a spherical particle is calculated, using the Thiele modulus for a first-order reaction according to Eq. (5).

$$\eta_{cat} = \frac{1}{\phi}\left(\frac{1}{\tanh(3\phi)} - \frac{1}{3\phi}\right) \tag{5}$$

For all hydrogenolysis experiments performed, the influence of the mass transport was dominated by the gas-liquid mass transfer. The overall catalyst efficiency for nearly all experiments was higher than 0.99. Only in some cases (experiments with a XYL concentration of 30 wt % or at low pressure: 20 bar) the corresponding overall catalyst efficiency was lower. However, even for the worst case (c_0: 1.972 mol$_{XYL}$L$_{sol}^{-1}$,

0.015 g$_{cat}$g$_{sol}^{-1}$, 0.06 g$_{Ca(OH)_2}$g$_{sol}^{-1}$, 170 °C, 80 bar) it was still higher than 0.97. Therefore, all measured data could be used for the estimation of the intrinsic reaction kinetics.

With regard to the availability of calcium hydroxide, the rate of dissolution of calcium hydroxide in water and the rate of consumption through neutralization reaction with the acids formed during XYL hydrogenolysis (LA, glycolic acid, formic acid, acetic acid, as well as carbon monoxide and dioxide) were compared. To ensure that a sufficient amount of base is dissolved at all times during the experiments, the rate of dissolution has to be significantly higher than the rate of acid formation. For the evaluation, the rate of acid formation was approximately described by a first-order rate law, while the solubility rate of calcium hydroxide was calculated analogously to a procedure known from the literature [45].

Comparing those data, it is obvious that the dissolution rate of calcium hydroxide (minimum 11.1×10^{-2} mol L^{-1}s^{-1} for c_0: 10 g$_{Ca(OH)_2}$L$_{sol}^{-1}$, 170 °C) is significantly higher than the rate of acid formation (maximum 68.0×10^{-6} mol L^{-1}s^{-1} for c_0: 1.972 mol$_{XYL}$L$_{sol}^{-1}$, 0.06 g$_{Ca(OH)_2}$g$_{sol}^{-1}$, 0.015 g$_{cat}$g$_{sol}^{-1}$, 170 °C, 80 bar). A limitation of the reactions during XYL hydrogenolysis by a shortage of dissolved solid base is therefore not to be expected. However, it has to be considered that the conditions under which the kinetic data for the calculation of the calcium hydroxide dissolution rate were measured are different from those under which XYL hydrogenolysis is performed. To make more precise statements about a possible limitation regarding the dissolution rate of the solid base, further investigations under the conditions of the hydrogenolysis experiments, i.e., high temperatures and pressures and in the presence of organic components, are necessary.

4.3 Estimation of the Kinetic Parameters

Since the partial pressures of the main products for XYL hydrogenolysis are small, gas-liquid equilibria were neglected. The evaporation of water was also not taken into account, since the evaporated water content from the liquid phase was well below 1.5 mol % in all cases. Since the proposed reaction network of XYL hydrogenolysis is quite complex (see Fig. 3), it was simplified as shown in Fig. 4.

Here, the minor components with low yields were not taken into account. These components include the carboxylic acids glycolic acid ($Y_i \leq 3.5$ mol %), formic acid, acetic acid ($Y_i \leq 3.0$ mol %) as well as the quantified alcohols ($Y_i \leq 3.0$ mol %) and the gaseous-phase components ($Y_i \leq 2.0$ mol %). These products are combined into a side component that is formed via subsequent reactions starting from EG, GLY, and XYL. In addition, these components compensate for the gap in the mass balance caused by unquantified species. Moreover, the equilibrium reaction between PG and LA was neglected. This is possible because both the yield of PG in LA hydrogenation ($Y_{PG} = 2.5$ mol %) and the yield of LA in PG hydrogenation ($Y_{LA} = 3.6$ mol %) are low.

The estimation of the kinetic parameters was carried out using gPROMS® (version 5.1.1) with the logarithmic likelihood function as objective function. To avoid dependencies between the kinetic parameters, in a first step, only the parameters of
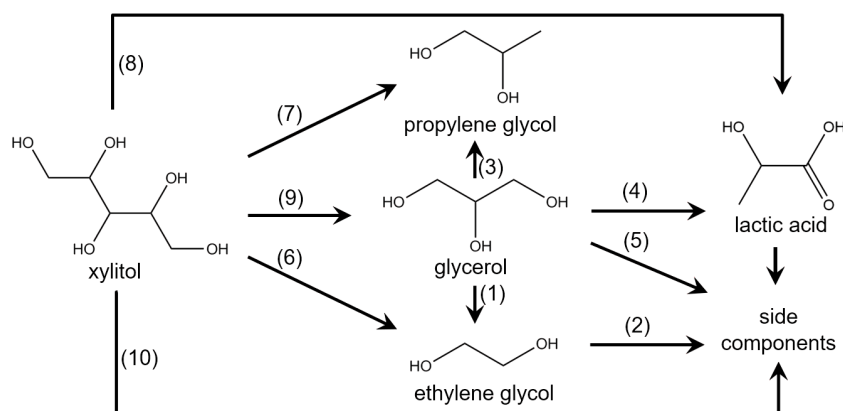
Figure 4. Reduced reaction network for the hydrogenolysis of XYL.

drogen are negative for all five reactions, which indicates an inhibition of the reaction rate by the dissolved hydrogen. Considering the reaction network shown in Fig. 3, it is obvious that dehydrogenation takes place in some of the reaction paths, which is favored under low hydrogen pressure.

The resulting fits for the concentration dependency (Fig. S8), the pressure dependency (Fig. S9), and the temperature dependency (Fig. S10) of GLY hydrogenolysis are shown in Sect. S4 of the Supporting Information. It is obvious that the stated kinetic model allows a good description of the measured concentration profiles. All of the components can be described with a deviation of less than 10 % from the measured values.

GLY hydrogenolysis were determined, which is a subnetwork of XYL hydrogenolysis. For the conversion of GLY to most of the products, simple power-law equations were used. Only for the kinetics of the reaction from GLY to LA, an additional hyperbolic term was used.

The obtained kinetic parameters are summarized in Tab. 3. It has to be noticed that the reaction orders with respect to hy-

The estimation of the kinetic parameters for XYL hydrogenolysis was carried out analogously to the estimation of the GLY kinetic parameters. Therefore, it is necessary to develop rate equations for the reactions in XYL hydrogenolysis in addition to the equations already developed for GLY hydrogenolysis (see Tab. 3). For the XYL kinetics, simple power-law equations were

Table 3. Rate equations and kinetic parameters for the aqueous-phase hydrogenolysis of GLY.

Equation	Parameter	Value
$r_1 = k_{0,1}\exp\left(-\dfrac{E_{a,1}}{RT}\right)c_{GLY}^{n_1}c_{H_2}^{m_{H_2,1}}$	$k_{0,1} \times 10^6 \left[L_{sol}^{(n_1+m_{H_2,1})}s^{-1}g_{cat}^{-1}mol^{(1-n_1-m_{H_2,1})}\right]$	33.0
	$E_{a,1}$ [kJ mol^{-1}]	128.9
	n_1 [–]	0.7
	$m_{H_2,1}$ [–]	−1.0
$r_2 = k_{0,2}\exp\left(-\dfrac{E_{a,2}}{RT}\right)c_{EG}^{n_2}c_{H_2}^{m_{H_2,2}}$	$k_{0,2} \times 10^6 \left[L_{sol}^{(n_2+m_{H_2,2})}s^{-1}g_{cat}^{-1}mol^{(1-n_2-m_{H_2,2})}\right]$	12.3
	$E_{a,2}$ [kJ mol^{-1}]	122.7
	n_2 [–]	1.2
	$m_{H_2,2}$ [–]	−1.5
$r_3 = k_{0,3}\exp\left(-\dfrac{E_{a,3}}{RT}\right)c_{GLY}^{n_3}c_{H_2}^{m_{H_2,3}}$	$k_{0,3} \times 10^6 \left[L_{sol}^{(n_3+m_{H_2,3})}s^{-1}g_{cat}^{-1}mol^{(1-n_3-m_{H_2,3})}\right]$	5.8
	$E_{a,3}$ [kJ mol^{-1}]	109.7
	n_3 [–]	1.0
	$m_{H_2,3}$ [–]	−0.8
$r_4 = k_{0,4}\exp\left(-\dfrac{E_{a,4}}{RT}\right)c_{GLY}^{n_4}c_{H_2}^{m_{H_2,4}}\left(\dfrac{1}{1+K_{LA,1}c_{LA}}\right)$	$k_{0,4} \times 10^6 \left[L_{sol}^{(n_4+m_{H_2,4})}s^{-1}g_{cat}^{-1}mol^{(1-n_4-m_{H_2,4})}\right]$	17.7
	$E_{a,4}$ [kJ mol^{-1}]	114.5
	n_4 [–]	0.7
	$m_{H_2,4}$ [–]	−0.8
	$K_{LA,1}$ [L mol^{-1}]	13.0
$r_5 = k_{0,5}\exp\left(-\dfrac{E_{a,5}}{RT}\right)c_{GLY}^{n_5}c_{H_2}^{m_{H_2,5}}$	$k_{0,5} \times 10^6 \left[L_{sol}^{(n_5+m_{H_2,5})}s^{-1}g_{cat}^{-1}mol^{(1-n_5-m_{H_2,5})}\right]$	4.4
	$E_{a,5}$ [kJ mol^{-1}]	144.4
	n_5 [–]	0.2
	$m_{H_2,5}$ [–]	−2.5

used, partly taking into account simple hyperbolic approaches. Inhibition via the LA concentration is appropriate as this is used in direct dependence on the concentration of calcium hydroxide in the liquid phase, which acts as a co-catalyst (see Fig. 3). A direct use of the base concentration was not possible due to missing measurement data. Furthermore, for these reactions, a term was used that describes the inhibition of the reaction rate due to the decreasing solubility concentration of the solid base with increasing temperature. It is necessary to take this aspect into account since it competes directly with an increase of the reaction rate via the Arrhenius law. The resulting kinetic parameters are summarized in Tab. 4.

For the kinetic parameters of the rate equations based on GLY, the corresponding parameter values (reaction orders n_i and $m_{H_2,i}$, $K_{LA,1}$) were used (see Tab. 3). This is valid because the conditions under which the respective experiments were performed are identical. In contrast, the pre-exponential factors and the activation energies have to be readjusted in the

Table 4. Rate equations and kinetic parameters for the aqueous phase hydrogenolysis of XYL.

Equation	Parameter	Value
$r_1 = k_{0,1}\exp\left(-\frac{E_{a,1}}{RT}\right)c_{GLY}^{n_1}c_{H_2}^{m_{H_2,1}}$	$k_{0,1}\times10^6\left[L_{sol}^{\left(n_1+m_{H_2,1}\right)}s^{-1}g_{cat}^{-1}mol^{\left(1-n_1-m_{H_2,1}\right)}\right]$	0
$r_2 = k_{0,2}\exp\left(-\frac{E_{a,2}}{RT}\right)c_{EG}^{n_2}c_{H_2}^{m_{H_2,2}}$	$k_{0,2}\times10^6\left[L_{sol}^{\left(n_2+m_{H_2,2}\right)}s^{-1}g_{cat}^{-1}mol^{\left(1-n_2-m_{H_2,2}\right)}\right]$	1.2
$r_3 = k_{0,3}\exp\left(-\frac{E_{a,3}}{RT}\right)c_{GLY}^{n_3}c_{H_2}^{m_{H_2,3}}$	$k_{0,3}\times10^6\left[L_{sol}^{\left(n_3+m_{H_2,3}\right)}s^{-1}g_{cat}^{-1}mol^{\left(1-n_3-m_{H_2,3}\right)}\right]$	3.2
$r_4 = k_{0,4}\exp\left(-\frac{E_{a,4}}{RT}\right)c_{GLY}^{n_4}c_{H_2}^{m_{H_2,4}}\left(\frac{1}{1+K_{LA,1}c_{LA}}\right)\left(1+K_{OH,1}c_{OH}\right)^{n_{OH,1}}$	$k_{0,4}\times10^6\left[L_{sol}^{\left(n_4+m_{H_2,4}\right)}s^{-1}g_{cat}^{-1}mol^{\left(1-n_4-m_{H_2,4}\right)}\right]$	0.2
$r_5 = k_{0,5}\exp\left(-\frac{E_{a,5}}{RT}\right)c_{GLY}^{n_5}c_{H_2}^{m_{H_2,5}}$	$k_{0,5}\times10^6\left[L_{sol}^{\left(n_5+m_{H_2,5}\right)}s^{-1}g_{cat}^{-1}mol^{\left(1-n_5-m_{H_2,5}\right)}\right]$	0
$r_6 = k_{0,6}\exp\left(-\frac{E_{a,6}}{RT}\right)c_{GLY}^{n_6}c_{H_2}^{m_{H_2,6}}\left(\frac{1}{1+K_{LA,2}c_{LA}}\right)\left(1+K_{OH,2}c_{OH}\right)^{n_{OH,2}}$	$k_{0,6}\times10^1\left[L_{sol}^{\left(n_6+m_{H_2,6}\right)}s^{-1}g_{cat}^{-1}mol^{\left(1-n_6-m_{H_2,6}\right)}\right]$	0.3
	$E_{a,6}$ [kJ mol^{-1}]	103.4
	n_6 [–]	0.5
	$m_{H_2,6}$ [–]	0.2
$r_7 = k_{0,7}\exp\left(-\frac{E_{a,7}}{RT}\right)c_{GLY}^{n_7}c_{H_2}^{m_{H_2,7}}\left(\frac{1}{1+K_{LA,2}c_{LA}}\right)\left(1+K_{OH,2}c_{OH}\right)^{n_{OH,2}}$	$k_{0,7}\times10^3\left[L_{sol}^{\left(n_7+m_{H_2,7}\right)}s^{-1}g_{cat}^{-1}mol^{\left(1-n_7-m_{H_2,7}\right)}\right]$	0.8
	$E_{a,7}$ [kJ mol^{-1}]	123.7
	n_7 [–]	0.5
	$m_{H_2,7}$ [–]	0.3
$r_8 = k_{0,8}\exp\left(-\frac{E_{a,8}}{RT}\right)c_{GLY}^{n_8}c_{H_2}^{m_{H_2,8}}\left(\frac{1}{1+K_{LA,2}c_{LA}}\right)\left(1+K_{OH,1}c_{OH}\right)^{n_{OH,1}}$ $\left(1+K_{OH,2}c_{OH}\right)^{n_{OH,2}}$	$k_{0,8}\times10^{-14}\left[L_{sol}^{\left(n_8+m_{H_2,8}\right)}s^{-1}g_{cat}^{-1}mol^{\left(1-n_8-m_{H_2,8}\right)}\right]$	0.7
	$E_{a,8}$ [kJ mol^{-1}]	0
	n_8 [–]	0.5
	$m_{H_2,8}$ [–]	0.2
$r_9 = k_{0,9}\exp\left(-\frac{E_{a,9}}{RT}\right)c_{GLY}^{n_9}c_{H_2}^{m_{H_2,9}}\left(\frac{1}{1+K_{LA,2}c_{LA}}\right)\left(1+K_{OH,2}c_{OH}\right)^{n_{OH,2}}$	$k_{0,9}\times10^3\left[L_{sol}^{\left(n_9+m_{H_2,9}\right)}s^{-1}g_{cat}^{-1}mol^{\left(1-n_9-m_{H_2,9}\right)}\right]$	0.3
	$E_{a,9}$ [kJ mol^{-1}]	123.7
	n_9 [–]	0.5
	$m_{H_2,9}$ [–]	0.1
$r_{10} = k_{0,10}\exp\left(-\frac{E_{a,10}}{RT}\right)c_{GLY}^{n_{10}}c_{H_2}^{m_{H_2,10}}\left(\frac{1}{1+K_{LA,2}c_{LA}}\right)\left(1+K_{OH,2}c_{OH}\right)^{n_{OH,2}}$	$k_{0,10}\times10^6\left[L_{sol}^{\left(n_{10}+m_{H_2,10}\right)}s^{-1}g_{cat}^{-1}mol^{\left(1-n_{10}-m_{H_2,10}\right)}\right]$	0.3
	$E_{a,10}$ [kJ mol^{-1}]	148.9
	n_{10} [–]	0.8
	$m_{H_2,10}$ [–]	0.1
	$n_{OH,1}$ [–]	2.0
	$n_{OH,2}$ [–]	4.8
	$K_{LA,2}$ [L mol^{-1}]	5.8
	$K_{OH,1}$ [L mol^{-1}]	1264.0
	$K_{OH,2}$ [L mol^{-1}]	2788.0

context of XYL kinetics. It should be noted that reactions (1) and (5) in Fig. 4, which result from the GLY conversion, are negligible for the XYL kinetics. Presumably, the rate of EG formation from GLY is significantly lower than the formation rate from XYL, resulting in negligible conversion of GLY to EG. Similarly, the formation of the side components from GLY (reaction (5) in Fig. 4) is negligible compared to the formation starting from XYL (reaction (10) in Fig. 4). It should also be noted that the activation energy for XYL conversion to LA is zero. On the one hand, the reaction rate is a function of the temperature and increases with rising temperature when the activation energy is positive (Arrhenius law). On the other hand, for the formation of LA from possible intermediates, a specific amount of the solid base has to be dissolved in the reaction solution. However, this solubility decreases significantly with increasing temperature. It is possible that the formation of LA is significantly inhibited at very low base concentrations, so that the increase in the reaction rate with increasing temperature appears to be negligible. It also has to

be noticed that the reaction orders with respect to hydrogen for the conversion of XYL are very small. Accordingly, no significant change in the concentration profiles is to be expected by varying the hydrogen pressure. A sequence of dehydrogenation, retro-aldol cleavage, and hydrogenation is frequently reported for the conversion of XYL [31, 41]. Referring to this reaction path, it can be assumed that the retro-aldol cleavage, which is catalyzed by the solid base, is the rate-determining step of the XYL conversion.

The resulting fit for the concentration dependency of XYL hydrogenolysis at 170 °C and 80 bar is exemplarily shown in Fig. 5. It is obvious that the stated kinetic model allows a good description of the measured concentration profiles. Especially the main species, XYL, EG, and PG, correspond well with the measured values (deviation of less than 10 %). For the majority of the LA concentrations, the deviation is also small (less than 10 %). Only at a reactant concentration of $1.314\,\mathrm{mol_{XYL}L_{sol}^{-1}}$ the deviations become larger, but are still less than 20 %.
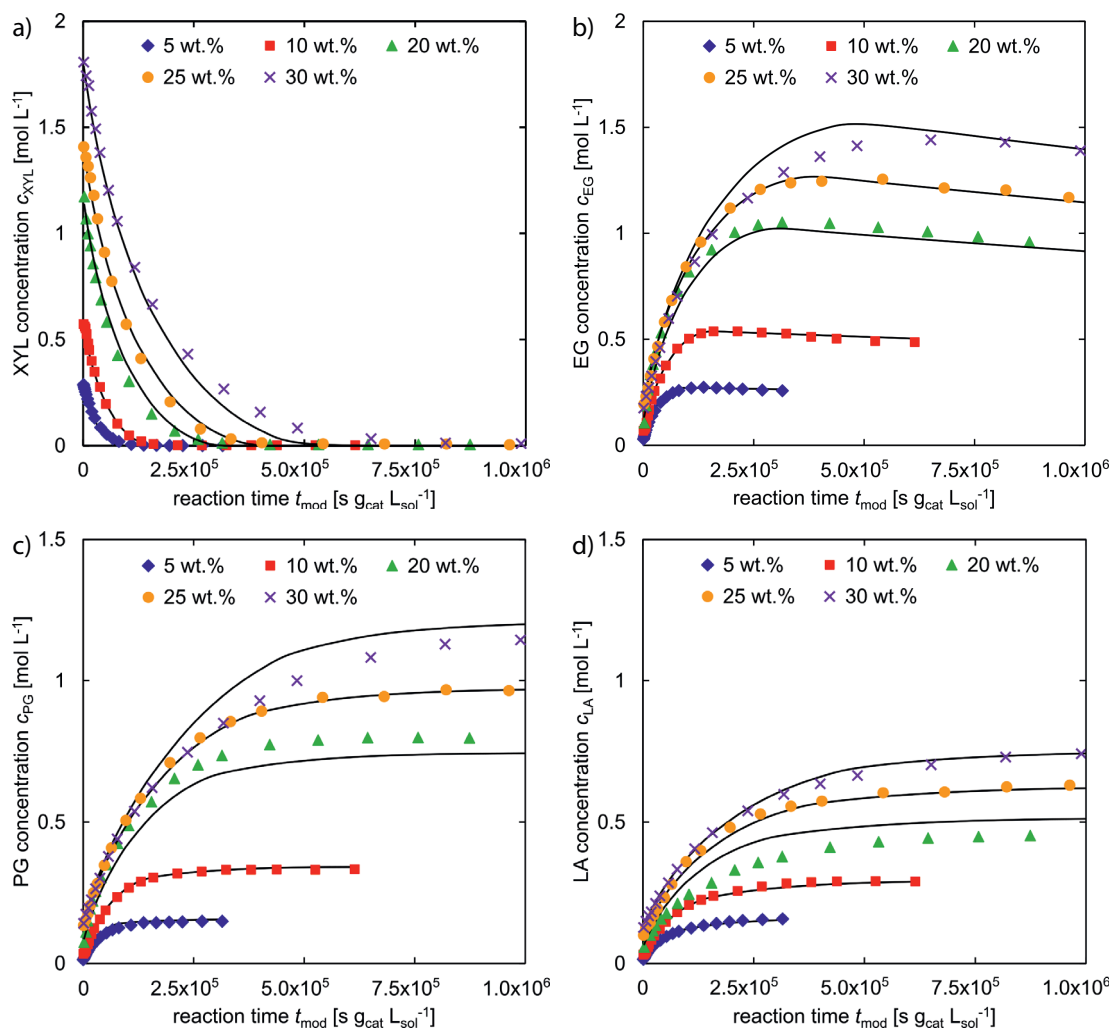
Figure 5. Measured (symbols) and calculated (lines) concentrations as a function of the modified time and the educt concentration during XYL hydrogenation (80 bar, 170 °C, $0.2\,\mathrm{g_{Ca(OH)_2}g_{XYL}^{-1}}$, $0.033\,\mathrm{g_{cat}g_{XYL}^{-1}}$). (a) XYL, (b) EG, (c) PG, (d) LA.

Moreover, the kinetic model provides a description of the pressure dependency (see Sect. S4 of the Supporting Information, Fig. S11) and the temperature dependency (see Sect. S4 of the Supporting Information, Fig. S12) with good accuracy, as the comparison between measured and calculated values shows.

Since EG and PG are of high economic interest, the sum of those yields are shown as a function of the modified time and in dependence on the temperature and XYL concentration in Fig. 6. It is obvious that an educt concentration of $1.314\,mol_{XYL}L_{sol}^{-1}$ is optimal for achieving the highest amounts of those glycols, whereby the total yield is approximately 67 mol %. Regarding the temperature dependency, it can be seen that a temperature of 190 °C is optimal to achieve the highest amount of glycols (Y_{EG+PG} approximately 68 mol %).

5   Conclusion

In the present work, the heterogeneously catalyzed hydrogenolysis of aqueous XYL solution to the valuable products EG and PG with LA and GLY as main by-products was investigated. Therefore, a 5 wt % platinum/activated carbon catalyst and calcium hydroxide as co-catalyst were used, which show good selectivities towards the glycols, with total yields of approximately 68 mol % at optimum reaction conditions. To determine the reaction network, systematic measurements with XYL and intermediate products were performed in a stirred-tank batch reactor. Based on these experiments, a reaction network with a variety of different reaction paths and products was developed. For the evaluation of the reaction kinetics as a function of the educt concentration, the pressure, and the temperature, the reaction network had to be simplified. This resulted in a reaction network for XYL hydrogenolysis consisting of ten reactions, taking into account the main products EG and PG as well as LA and GLY, whereby all other products were combined

to a single side component. It was ensured that the intrinsic kinetics was measured in all cases through the assessment of mass transport limitations. By selecting suitable kinetic approaches, it was possible to describe the influence of the most important reaction conditions on the measured concentration profiles with good accuracy. By using this quantitative description of the reaction network, an optimal educt concentration of $1.314\,mol_{XYL}L_{sol}^{-1}$ and an optimal reaction temperature of 190 °C could be determined. As a result, the determined reaction kinetics provides a good basis for designing suitable reactor concepts for industrial production of bio-derived EG and PG in the next step.
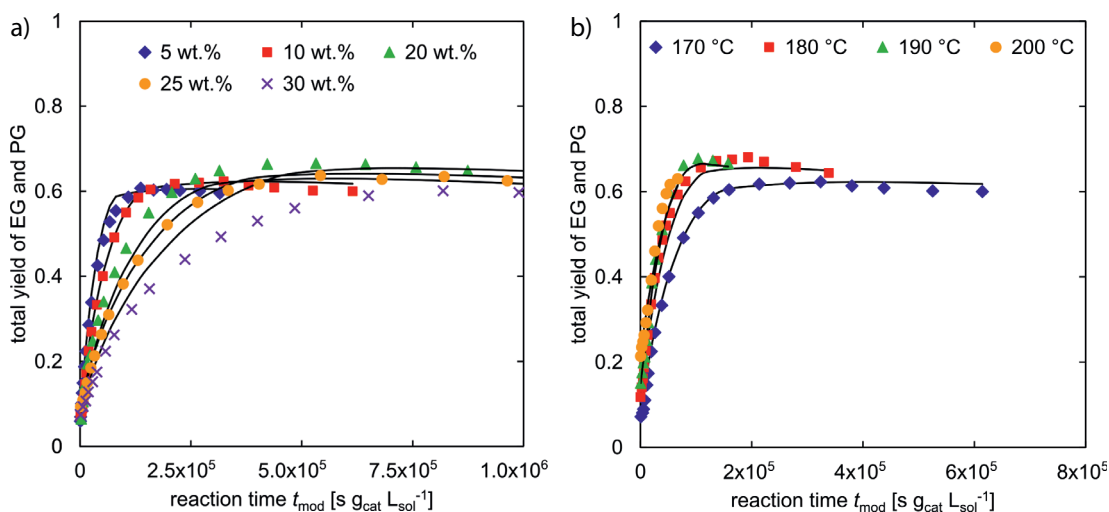
Supporting Information

Acknowledgment

The authors have declared no conflict of interest.

Figure 6. Measured (symbols) and calculated (lines) data of (a) the total yield of main products (EG and PG) for various concentrations at 80 bar, 170 °C, and (b) the total yield of main products (EG and PG) for various temperatures at 80 bar, $0.657\,mol_{XYL}L_{sol}^{-1}$ ($0.2\,g_{Ca(OH)_2}g_{XYL}^{-1}$, $0.033\,g_{cat}g_{XYL}^{-1}$).

Symbols used

c	$[\text{mol L}^{-1}]$	concentration
E_a	$[\text{J mol}^{-1}]$	activation energy
k	$\left[\text{L}_{\text{sol}}^{(n_i+m_{H_2,j})}\text{s}^{-1}\text{g}_{\text{cat}}^{-1}\text{mol}^{(1-n_i-m_{H_2,j})}\right]$ reaction rate constant	
k_0	$\left[\text{L}_{\text{sol}}^{(n_i+m_{H_2,j})}\text{s}^{-1}\text{g}_{\text{cat}}^{-1}\text{mol}^{(1-n_i-m_{H_2,j})}\right]$ frequency factor	
K_i	$[-]$	rate constant for the inhibition of reactions
m	$[\text{g}]$	mass
$m_{H_2,j}$	$[-]$	reaction order with respect to the concentration of hydrogen in reaction j
n	$[\text{mol}]$	amount of substance
$n_{i,j}$	$[-]$	reaction order with respect to the concentration of component i in reaction j
p	$[\text{bar}]$	pressure
R	$[\text{J mol}^{-1}\text{K}^{-1}]$	universal gas constant
r_j	$[\text{mol s}^{-1}\text{g}_{\text{cat}}^{-1}]$	rate of reaction j
t	$[\text{s}]$	time
T	$[\text{K}]$	temperature
t_{mod}	$[\text{s g}_{\text{cat}}\text{L}_{\text{sol}}^{-1}]$	modified time
V	$[\text{L}]$	volume
x_{50}	$[\mu\text{m}]$	mass-median radius
Y_i	$[\text{mol mol}^{-1}]$	yield of component i

Greek letters

β	$[-]$	number of carbon atoms
ν	$[-]$	stoichiometric coefficient
ρ	$[\text{kg m}^{-3}]$	density

Sub- and superscripts

cat	catalyst
e	educt
H_2	hydrogen
mod	modified
p	product
sol	solution

Abbreviations

EG	ethylene glycol
FID	flame ionization detector
GC	gas chromatography
GLY	glycerol
HPLC	high-performance liquid chromatography
LA	lactic acid
PG	propylene glycol
UV	ultraviolet
XYL	xylitol

References

[1] M. Paster, J. L. Pellegrino, T. M. Carole, *Industrial Bioproducts: Today and Tomorrow*, Energetics, Inc., Columbia, MD **2003**.

[2] *Statistical Review of World Energy*, BP p.l.c., London **2017**. www.bp.com/en/global/corporate/energy-economics/statistical-review-of-world-energy.html

[3] M. J. Climent, A. Corma, S. Iborra, *Green Chem.* **2011**, *13 (3)*, 520. DOI: https://doi.org/10.1039/c0gc00639d

[4] H. Yue, Y. Zhao, X. Ma, J. Gong, *Chem. Soc. Rev.* **2012**, *41 (11)*, 4218–4244. DOI: https://doi.org/10.1039/c2cs15359a

[5] Ethylene Glycols, in *Chemical Economics Handbook*, IHS Markit, London **2018**. https://ihsmarkit.com/products/ethylene-glycols-chemical-economics-handbook.html

[6] Propylene Glycols, *Chemical Economics Handbook*, IHS Markit, London **2017**. https://ihsmarkit.com/products/propylene-oxide-chemical-economics-handbook.html

[7] S. Rebsdat, D. Mayer, Ethylene Oxide, in *Ullmann's Encyclopedia of Industrial Chemistry*, Wiley-VCH, Weinheim **2001**. DOI: https://doi.org/10.1002/14356007.a10_117

[8] S. Rebsdat, D. Mayer, Ethylene Glycol, in *Ullmann's Encyclopedia of Industrial Chemistry*, Wiley-VCH, Weinheim **2000**. DOI: https://doi.org/10.1002/14356007.a10_101

[9] H. Baer, M. Bergamo, A. Forlin, L. H. Pottenger, J. Lindner, Propylene Oxide, in *Ullmann's Encyclopedia of Industrial Chemistry*, Wiley-VCH, Weinheim **2012**. DOI: https://doi.org/10.1002/14356007.a22_239.pub3

[10] C. J. Sullivan, Propanediols, in *Ullmann's Encyclopedia of Industrial Chemistry*, Wiley-VCH, Weinheim **2018**. DOI: https://doi.org/10.1002/14356007.a22_163.pub2

[11] C. A. G. Quispe, C. J. R. Coronado, J. A. Carvalho Jr., *Renewable Sustainable Energy Rev.* **2013**, *27*, 475–493. DOI: https://doi.org/10.1016/j.rser.2013.06.017

[12] H. Lieth, R. H. Whittaker, *Primary Productivity of the Biosphere*, Ecological Studies 14, Springer, Berlin **1975**.

[13] A. M. Ruppert, K. Weinberg, R. Palkovits, *Angew. Chem.* **2012**, *51 (11)*, 2564–2601. DOI: https://doi.org/10.1002/anie.201105125

[14] C. Glotzbach, S. Schirrmeister, R. Palkovits, P. J. C. Hausoul, A. K. Beine, *Patent DE 102017204322 A1*, **2017**.

[15] *Chemicals and Fuels from Bio-Based Building Blocks* (Eds: F. Cavani, S. Albonetti, F. Basile, A. Gandini), Vol. 1, John Wiley & Sons, New York **2016**.

[16] X. Wang, A. K. Beine, R. Palkovits, in *Horizons in Sustainable Industrial Chemistry and Catalysis* (Eds: S. Albonetti, S. Perathoner, E. A. Quadrelli), Studies in Surface Science and Catalysis, Vol. 178, Elsevier, Amsterdam **2019**.

[17] A. Tullo, *C&EN* **2017**, *95 (46)*, 10. DOI: https://doi.org/10.1021/cen-09546-notw6

[18] *Bio-MEG Demoplant Avantium to be Located in Delfzijl*, Agro & Chemistry, 's-Hertogenbosch, The Netherlands **2019**. www.agro-chemistry.com/news/bio-meg-demoplant-avantium-to-be-located-in-delfzijl/

[19] *Avantium*, press release, Kunststoff Information Verlagsgesellschaft mbH, Bad Homburg **2019**. www.plasteurope.com/news/AVANTIUM_t242135/

[20] *UPM investiert in Biochemikalienproduktion der Zukunft am Standort Leuna*, UPM Media Relations, Leuna **2020**.

[21] H. Liu, Z. Huang, C. Xia, Y. Jia, J. Chen, H. Liu, *ChemCatChem* **2014**, *6 (10)*, 2918–2928. DOI: https://doi.org/10.1002/cctc.201402141

[22] Z. Huang, J. Chen, Y. Jia, H. Liu, C. Xia, H. Liu, *Appl. Catal., B* **2014**, *147*, 377–386. DOI: https://doi.org/10.1016/j.apcatb.2013.09.014

[23] T. Soták, T. Schmidt, M. Hronec, *Appl. Catal., A* **2013**, *459*, 26–33. DOI: https://doi.org/10.1016/j.apcata.2013.04.006

[24] R. Ooms, M. Dusselier, J. A. Geboers, B. op de Beeck, R. Verhaeven, E. Gobechiya, J. A. Martens, A. Redl, B. F. Sels, *Green Chem.* **2014**, *16 (2)*, 695–707. DOI: https://doi.org/10.1039/C3GC41431K

[25] J. Sun, H. Liu, *Green Chem.* **2011**, *13 (1)*, 135–142. DOI: https://doi.org/10.1039/C0GC00571A

[26] S. P. Chopade, D. J. Miller, J. E. Jackson, J. G. Frye, A. H. Zacher, *US Patent 6291725 B1*, **2000**.

[27] J. Lee, Y. Xu, G. W. Huber, *Appl. Catal., B* **2013**, *140–141*, 98–107. DOI: https://doi.org/10.1016/j.apcatb.2013.03.031

[28] Z. Zhou, S. Dai, J. Qin, P. Yu, W. Wu, *RSC Adv.* **2015**, *5 (86)*, 70410–70416. DOI: https://doi.org/10.1039/C5RA08472E

[29] X. Jin, D. Roy, P. S. Thapa, B. Subramaniam, R. V. Chaudhari, *ACS Sustainable Chem. Eng.* **2013**, *1 (11)*, 1453–1462. DOI: https://doi.org/10.1021/sc400189d

[30] K. L. Deutsch, D. G. Lahr, B. H. Shanks, *Green Chem.* **2012**, *14 (6)*, 1635. DOI: https://doi.org/10.1039/c2gc00026a

[31] M. Rivière, N. Perret, A. Cabiac, D. Delcroix, C. Pinel, M. Besson, *ChemCatChem* **2017**, *9 (12)*, 2145–2159. DOI: https://doi.org/10.1002/cctc.201700034

[32] A. K. Beine, A. J. D. Krüger, J. Artz, C. Weidenthaler, C. Glotzbach, P. J. C. Hausoul, R. Palkovits, *Green Chem.* **2018**, *20 (6)*, 1316–1322. DOI: https://doi.org/10.1039/C8GC00208H

[33] M. Rivière, N. Perret, D. Delcroix, A. Cabiac, C. Pinel, M. Besson, *ACS Sustainable Chem. Eng.* **2018**, *6 (3)*, 4076–4085. DOI: https://doi.org/10.1021/acssuschemeng.7b04424

[34] R. V. Chaudhari, A. Torres, X. Jin, B. Subramaniam, *Ind. Eng. Chem. Res.* **2013**, *52 (44)*, 15226–15243. DOI: https://doi.org/10.1021/ie400709d

[35] X. Jin, J. Shen, W. Yan, M. Zhao, P. S. Thapa, B. Subramaniam, R. V. Chaudhari, *ACS Catal.* **2015**, *5 (11)*, 6545–6558. DOI: https://doi.org/10.1021/acscatal.5b01324

[36] H. Liu, Z. Huang, H. Kang, X. Li, C. Xia, J. Chen, H. Liu, *Appl. Catal., B* **2018**, *220*, 251–263. DOI: https://doi.org/10.1016/j.apcatb.2017.08.022

[37] T. A. Werpy, J. G. Frye, A. H. Zacher, D. J. Miller, *US Patent 6479713 B1*, **2001**.

[38] *Catalysis of Organic Reactions* (Ed: J. R. Sowa Jr.), CRC Press, Boca Raton, FL **2005**.

[39] A. B. Miller, M. Raghunath, V. Sokolovskii, C. G. Lugmair, A. F. Volpe Jr., W. Shen, W. Turbeville, *US Patent 9 205 412 B2*, **2013**.

[40] C. Heisig, J. Diedenhoven, C. Jensen, H. Gehrke, T. Turek, *Chem. Eng. Technol.* **2020**, *43 (3)*, 484–492.

[41] A. K. Beine, *Ph.D. Thesis*, RWTH Aachen **2019**.

[42] H. Schäfer, *Ph.D. Thesis*, Friedrich-Alexander-Universität Erlangen-Nürnberg **2005**.

[43] L. B. Yeatts, W. L. Marshall, *J. Phys. Chem.* **1967**, *71 (8)*, 2641–2650. DOI: https://doi.org/10.1021/j100867a038

[44] *Lime: The Versatile Chemical: Properties of Typical Commercial Lime Products*, Fact Sheet, National Lime Association, Arlington, VA **2007**.

[45] K. Johannsen, S. Rademacher, *Acta Hydrochim. Hydrobiol.* **1999**, *27 (2)*, 72–78. DOI: https://doi.org/10.1002/(SICI)1521-401X(199902)27:2<72::AID-AHEH72>3.0.CO;2-H